Catena 123 (2014) 121–134

Contents lists available at ScienceDirect

Catena

journal homepage: www.elsevier.com/locate/catena

Weathering assessment in the Achala Batholith of the Sierra de Comechingones, Córdoba, central Argentina. I: Granite–regolith fractionation

V.A. Campodonico *, J.O. Martínez, S.O. Verdecchia, A.I. Pasquini, P.J. Depetris

Centro de Investigaciones en Ciencias de la Tierra (CICTERRA), Consejo Nacional de Investigaciones Científicas y Técnicas (CONICET), Universidad Nacional de Córdoba, Av. Vélez Sarsfield 1611, X5016CGA Córdoba, Argentina

ARTICLE INFO

Article history:
Received 6 December 2013
Received in revised form 7 July 2014
Accepted 23 July 2014
Available online xxxx

Keywords:
Weathering-limited
Granitic environment
Rare earth elements
Sorting

ABSTRACT

Weathering assessment in a *weathering-limited* environment is a difficult task because a significant proportion of the regolith has been removed by tectonically-induced denudation. In such an environment, the remnants of the altered mineral debris must be studied with care in order to attain a meaningful picture of the rate and intensity of ongoing weathering. A monolithologic (i.e., granite), small (~2 km^2), and mountainous (~1500 m elevation) drainage basin in the Sierras de Comechingones (31°54′07″S 64°45′28″W–31°53′11″S 64°44′16″W, Córdoba, central Argentina) was selected as a pilot area to survey the nature of weathering in a *weathering-limited* erosional setting, and a semiarid climatic regime. A relatively thin-layered, coarse-grained regolith and scattered sediment (i.e., fine-grained regolith) that had accumulated in valleys and topographic depressions were analyzed. The most abundantly identified clay mineral in the regolith is illite followed by kaolinite > smectite. Smectite seems to be the only clay mineral clearly associated with weathering. Petrographic observations and geochemical analyses, supported by statistical tests, define chemical weathering as incipient. Petrography indicates that plagioclase and biotite are the main mineral phases affected by alteration, which is more intense in the fine-grained regolith. Coarse- and fine-grained regoliths are chemically similar, among them and with the country rock, with statistically significant losses in the fine fraction of MgO, MnO and P_2O_5. Depletions of trace elements and REE, which are best explained by sorting than by actual rock alteration, are not statistically significant. Ternary diagrams reveal that the masses of Al_2O_3, CaO, Na_2O and K_2O were not significantly altered during weathering and transportation, and that regolith samples correspond to a coarse residue relatively enriched in feldspars (and quartz), where the mud-fraction (with high clay mineral contents) has been removed from the drainage basin by high-energy processes.

© 2014 Elsevier B.V. All rights reserved.

1. Introduction

Rock alteration on the Earth's surface is a major link in the complex chain that relates different spheres (i.e., hydrosphere, atmosphere, lithosphere and biosphere). Therefore, rock breakdown (i.e., *weathering*) plays a significant role in, for example, climate control. The Berner, Lassaga and Garrels (Berner et al., 1983) hypothesis along with the tectonic forcing model of Raymo and Ruddiman (1992) are clear examples of the complex interplay between global climate and rock weathering. Chemical weathering of crystalline silicate rocks, for example, is considered to be the main factor controlling the consumption of atmospheric CO_2 at a geological scale (e.g., Berner, 1992).

The term *weathering* is used in the Earth Sciences to denote the in situ breakdown and alteration of rocks and minerals. In the near surface environment, pressure, temperature and water availability differs significantly from those prevailing at the crust's interior. Because of this disequilibrium, exposed rocks are easily attacked, decomposed, and eroded by various chemical and physical surface processes (e.g., Pope, 2013; Viles, 2013, and references therein). The term weathering conveys, as well, a close linkage with atmospheric conditions (i.e., weather) (e.g., Hall et al., 2012). At any rate, weathering involves a set of processes that prepare rock material for transport, and such movable debris or *regolith* is defined as "the mantle of in situ and transported material that covers the landscapes across the world" (Scott and Pain, 2009).

Carson and Kirkby (1972) identified two distinctive erosional regimes: one is known as *transport-limited*, and the other as *weathering-limited*. Stallard and Edmond (1983), in their analysis of the dynamics of weathering in the Amazon, recognized that weathering-limited environments are characterized by little or no soil development, and as a result sediment derived from such source areas is relatively unaltered.

The assessment of weathering intensity and rate in a transport-limited regime is a relatively straightforward process because the

* Corresponding author. Tel.: +54 351 5353800.
E-mail address: vcampodonico@efn.uncor.edu (V.A. Campodonico).

http://dx.doi.org/10.1016/j.catena.2014.07.016
0341-8162/© 2014 Elsevier B.V. All rights reserved.

existence of thick, well-developed weathering profiles allows the use of various methodologies, such as the so-called "absolute" approach, through the "benchmark mineral" method (e.g., Krauskopf and Bird, 1995) or a myriad of relative indices, like the chemical index of alteration (CIA, Nesbitt and Young, 1982), the chemical index of weathering (CIW, Harnois, 1988), and other similar ratios (e.g., Depetris et al., 2014). The evaluation of weathering is more difficult in a weathering-limited scenario because a significant part – if not all – of the regolith has been removed and the landscape is composed of bare exposed rocks and patches of relatively thin regolith and accumulated sediment and/or incipient soil development. For these reasons, there are relatively few studies that have probed into the nature of weathering in semi-arid, mostly weathering-limited environments, such as those prevailing in Argentina's Sierras Pampeanas. In this region, a relevant example is the work of Román-Ross et al. (1998), who surveyed the chemical and mineralogical changes that occur in association with the weathering of the Achala Batholith. Kirschbaum et al. (2005) produced one of the few weathering studies in the Sierra Norte of Córdoba (Argentina), examining a poorly developed weathering profile on granitic basement, within a more regional framework than the one used in this paper.

In this contribution we compare the original country rock with the overlying regolith, seeking to establish relative gains and losses of major and trace elements (including REE) that granite undergoes in a small and typical weathering-limited drainage basin in the Achala Batholith (Sierra de Comechingones, Córdoba Province, Argentina, Fig. 1A and B). In so doing we seek to determine a stepping stone that will allow us to probe further into the nature of weathering in this region.

This work is the first part of an integral study of weathering assessment in a pilot area of the Achala Batholith. The inspection of dissolved geochemistry and its implication in weathering will constitute the bulk of the next contribution.

2. Geological setting and climate characterization of the study area

The small analyzed drainage basin (~2 km^2), herein known as "La Trucha" (Spanish for The Trout), is located in the southern portion of the Achala Batholith, within the Sierra de Comechingones (Fig. 1). The Sierra de Comechingones is one of the southernmost ranges of the Sierras Pampeanas in central Argentina, which consist of Paleozoic basement blocks bounded by faults (González Bonorino, 1950) and uplifted as a result of Cenozoic Andean compression (Isacks, 1988; Jordan and Allmendinger, 1986). The Sierra de Comechingones is mainly composed of Early Cambrian middle- to high-grade metamorphic rocks and Cambrian to Devonian granites (Gordillo, 1984; Otamendi et al., 1999; Rapela et al., 1998, 2008; Siegesmund et al., 2010). These basement rocks are unconformably overlain by unconsolidated Early Cenozoic sediments (e.g., Bonalumi et al., 1998).

The Achala Batholith, with a surface area of ~2500 km^2, is the largest of a series of granitic intrusive bodies in the eastern Sierras Pampeanas, which are discordant to structural features and metamorphic and igneous rocks of early Paleozoic age. The contact aureoles of this body indicate a shallow emplacement, usually less than 2 kbar (e.g., Pinotti et al., 2002), while available U–Pb ages suggest a Late Devonian age (e.g., Dorais et al., 1997; Rapela et al., 2008). The granites of the Achala Batholith have SiO_2 contents between 60% and 76% and are termed aluminous A-type granites (Rapela et al., 2008 and references therein). Lira and Kirschbaum (1990) described five petro-facies within the batholith. Facies A is a monzo-leucogranite that occurs near the margin of

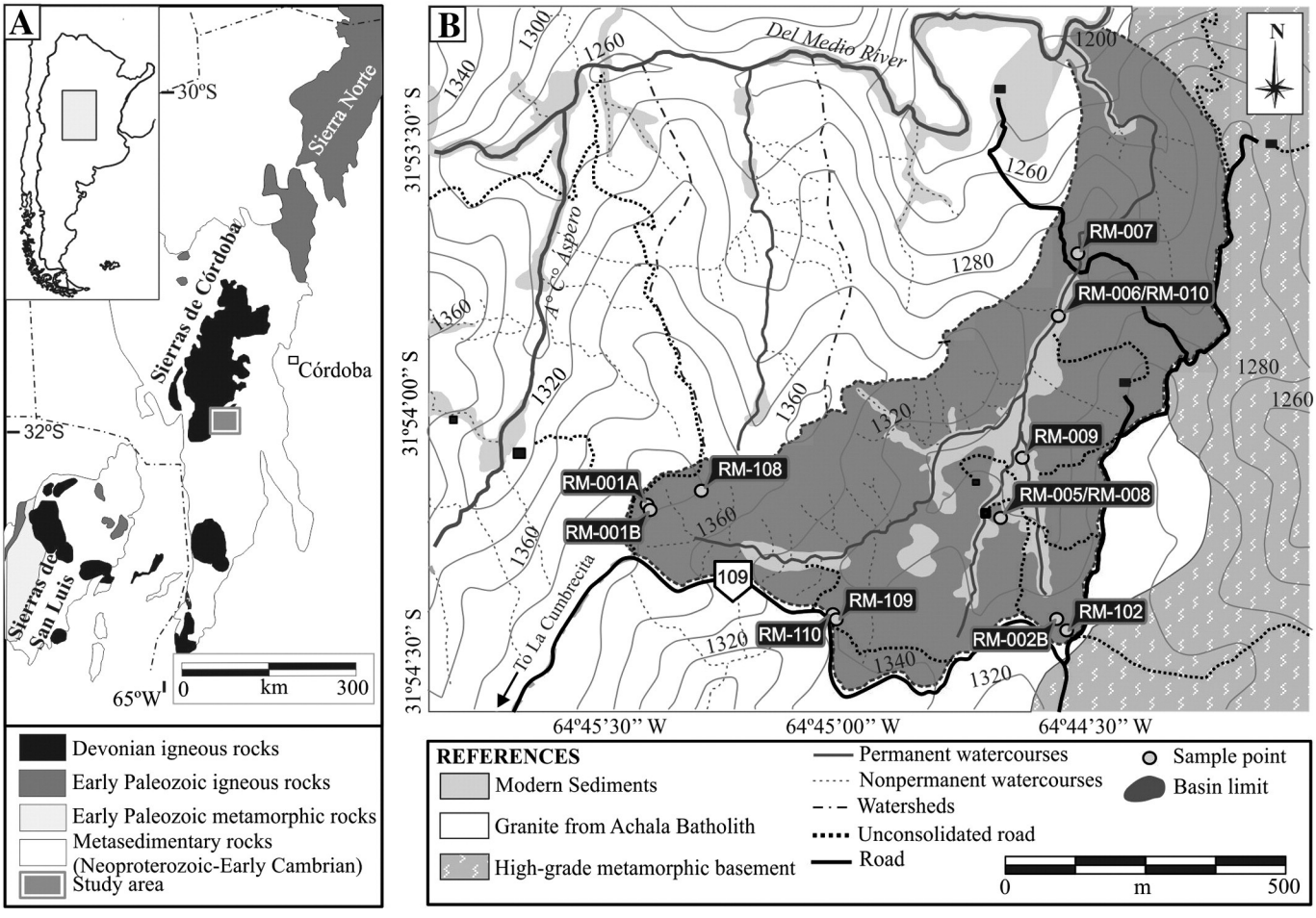

Fig. 1. A) Location of the study area (modified from Siegesmund et al., 2010). B) Schematic geological map of the La Trucha drainage basin and the location of sampling sites.

the batholith; Facies B is a porphyritic monzogranite with K-feldspar megacrysts and is the dominant facies of the batholith (it is the only facies that was recognized in the studied drainage basin); Facies C is a fine-grained monzogranite with scarce K-feldspar megacrysts; Facies D is a fine-grained monzogranite without K-feldspar megacrysts; and Facies E is a fine-grained monzogranite with biotite clots. The main mineral assemblage is quartz, microcline, plagioclase (An_{2-22}), biotite, and muscovite, with several accessory minerals (Lira and Kirschbaum, 1990). An extensive late magmatic/deuteric event produced muscovitization of biotite, and sometimes of feldspars, albitization of K-feldspar and plagioclase, and the formation of nodules with black tourmaline nuclei and silica enriched haloes, associated with the alteration of feldspars and biotite (e.g., Demange et al., 1996; Lira and Kirschbaum, 1990). Muscovitization occurs on a regional scale, while the other processes are restricted to Facies A.

Very limited accumulations of fluvial (autochthonous) and loess-like sediments (allochthonous) are present in the highest part of the region underlain by the batholith.

The main geomorphological feature of the Achala Batholith is the presence of bornhardts and high plains (locally known as “pampas de altura”, at ~2000 m elevation). This landscape with rounded granite blocks is interpreted as the remnant of deep paleoweathering, whereas the high plains represent an erosional paleosurface (Rabassa et al., 1996) (Fig. 2).

Carignano et al. (1999) proposed a morphogenic evolution for the erosional surfaces of the Sierras Pampeanas. During the great Gondwana glaciation of Middle Carboniferous times, the Sierras Pampeanas underwent erosional denudation, mainly due to the action of large alpine-type glaciers. During Jurassic times, a long period of quiescence and a humid tropical climate enabled the development of a broad planation surface. The occurrence of corestones and bornhardts are interpreted as residual landforms developed during this period. Each major pulse of continental rifting during Late Jurassic–Late Cretaceous times generated an erosional cycle and the development of two planation surfaces. Similar cycles continued into the Miocene. Almost all planation surfaces have been broken and tilted during the Cenozoic Andean compression that uplifted the Sierras Pampeanas. Thick and mature Quaternary calcretes remain as evidence of long-term stable conditions.

The last stage of uplift and deformation of the Sierras Pampeanas is interpreted to be closely related to the Andean flat-slab subduction of the Nazca plate beneath the South American plate. Total exhumation rate in the Sierra the Comechingones since the Late Cretaceous is estimated by Lobens et al. (2011) to be ~2.3 km.

The small studied watershed (31°54′07″S 64°45′28″W–31°53′11″S 64°44′16″W, ~1400 m elevation) is part of the Río del Medio drainage basin (Fig. 1). It is underlain by the Achala Batholith (Facies B), and modern sediments generally fill the rivers' floodplain. “La Trucha” is 3500 m long and its drainage network is strongly controlled by the fracture pattern of the batholith.

The study area lies in Argentina's temperate zone, which is characterized by active atmospheric dynamics and the action of polar and subpolar fronts. The climate in the region is typically continental, and the irregular annual precipitation is a distinctive feature. In austral winter, climate is controlled by dominating action centers and access of humid Atlantic air is slowed down, thus generating a dry season. In contrast, rainfall increases in summer and in early autumn, mainly due to humid air coming in from the north (Capitanelli, 1979; Pasquini et al., 2006). As a consequence, about 75% of the total annual precipitation (~1060 mm, for the period 1943–2004) occurs between November and March. During the wet season the mean monthly rainfall is ~160 mm, whereas in the dry period (April–September) is ~40 mm.

According to Capitanelli (1979), the study area is framed within the annual mean isotherm of 16 °C, dropping to about 10 °C at 2000 m elevation. The maximum mean isotherm is 20 °C, whereas in the higher areas is about 14 °C. On the other hand, for the lowermost areas, the minimum mean isotherm is 9 °C, while it is about 5 °C for the highest ones.

Fig. 2. Typical landscape of Sierra de Comechingones. View is looking north, in the downstream direction at La Trucha drainage basin. Notice exposed, rounded granite blocks of the Achala Batholith. The width at the bottom of the photograph is ~4 m.

Table 1
Bulk chemical (major, trace and rare earth elements) and mineralogical composition of the granite country rock, and coarse- and fine-grained regolith samples of "La Trucha" watershed at the Achala Batholith. Samples of Achala Batholith and Pampean loess are also included.

	Granite				Coarse-grained regolith			Fine-grained regolith					Bed sed.	Achala Batholith		Loess	
Sample	RM102	RM001A	RM109	RM110	RM108	RM001B	RM002B	RM005	RM006	RM008	RM009	RM010	RM007	ACH-135[1]	S5[2]	A[3]	C[4]
wt.%																	
SiO_2	74.97	70.63	68.95	70.43	72.27	69.54	70.52	76.30	72.80	73.84	71.25	72.97	70.93	70.86	70.58	62.47	61.30
Al_2O_3	13.85	14.95	14.70	15.36	14.69	15.52	15.81	12.54	14.13	13.69	14.47	13.64	15.38	14.22	15.21	13.32	15.4
$Fe_2O_{3(T)}$	1.65	1.76	3.24	2.62	1.24	2.58	2.04	1.05	2.06	1.25	2.16	1.95	2.25	3.06	1.93	4.31	4.83
MnO	0.04	0.039	0.05	0.041	0.02	0.04	0.04	0.02	0.02	0.02	0.03	0.03	0.04	0.05	0.02	0.08	
MgO	0.40	0.50	0.80	0.71	0.27	0.63	0.50	0.19	0.40	0.25	0.43	0.38	0.53	0.47	0.49	1.74	1.87
CaO	1.12	0.63	1.35	1.10	0.72	1.20	1.11	0.58	0.82	0.70	0.78	0.73	1.22	1.53	1.15	4.82	4.45
Na_2O	3.11	2.38	2.70	2.87	2.52	3.01	3.04	2.42	2.73	2.64	2.86	2.67	3.56	2.88	3.21	2.49	4.62
K_2O	3.94	6.12	5.57	5.96	6.88	5.42	6.45	5.61	4.40	5.60	4.40	4.59	4.16	5.41	4.93	2.58	2.33
TiO_2	0.21	0.35	0.62	0.42	0.17	0.41	0.32	0.17	0.40	0.20	0.40	0.35	0.43	0.42	0.30	0.65	0.70
P_2O_5	0.19	0.29	0.33	0.24	0.20	0.25	0.21	0.12	0.09	0.14	0.09	0.10	0.17	0.17	0.25	0.16	0.17
LOI	0.65	1.11	0.93	0.93	0.74	1.26	0.81	0.66	2.15	1.57	2.46	2.93	1.72	0.41	1.41	7.26	4.45
ppm																	
Sc	3.00	3.00	4.00	3.00	2.00	3.00	3.00	1.00	4.00	2.00	4.00	4.00	4.00		3.00	11.00	
Be	7.00	11.00	4.00	6.00	7.00	8.00	8.00	5.00	11.00	6.00	10.00	8.00	10.00			4.00	
V	16.00	70.00	53.00	37.00	15.00	33.00	23.00	12.00	34.00	16.00	36.00	30.00	32.00		28.30	81.00	
Cr	90.00	50.00	50.00	80.00	100.00	90.00	70.00	80.00	80.00	130.00	80.00	130.00	70.00		<20.00	30.00	
Co	2.00	2.00	5.00	4.00	1.00	4.00	3.00	1.00	2.00	1.00	3.00	3.00	3.00		3.00	10.00	
Ni	<20.00	<20.00	<20.00	<20.00	<20.00	<20.00	<20.00	<20.00	<20.00	<20.00	<20.00	<20.00	<20.00		<20.00	<20.00	
Cu	20.00	10.00	30.00	20.00	10.00	20.00	10.00	<10.00	10.00	<10.00	10.00	<10.00	10.00		39.40	30.00	
Zn	50.00	50.00	110.00	90.00	<30.00	70.00	50.00	<30.00	40.00	<30.00	40.00	40.00	60.00		20.60	90.00	
Ga	24.00	25.00	30.00	26.00	21.00	26.00	23.00	17.00	21.00	19.00	22.00	20.00	25.00	23.00	21.70	19.00	
Ge	1.80	2.70	1.90	1.80	1.50	1.60	1.60	1.40	1.70	1.40	1.70	1.70	1.70			2.00	
As	<5.00	8.00	<5.00	<5.00	<5.00	<5.00	<5.00	<5.00	<5.00	<5.00	<5.00	<5.00	<5.00		<5.00	11.00	16.70
Rb	286.00	516.00	359.00	333.00	362.00	309.00	324.00	277.00	257.00	280.00	252.00	250.00	266.00	281.00	306.00	111.00	
Sr	94.00	132.00	138.00	159.00	158.00	164.00	179.00	145.00	161.00	157.00	154.00	152.00	150.00	133.00	102.00	304.00	
Y	8.90	13.70	14.90	11.60	7.50	12.70	13.20	5.00	13.10	6.40	11.80	10.60	9.30	21.40	11.60	28.00	
Zr	105.00	252.00	449.00	241.00	108.00	222.00	182.00	114.00	203.00	131.00	218.00	190.00	179.00	406.00	153.00	258.00	
Nb	18.10	29.40	33.60	21.40	12.00	21.60	18.70	10.50	20.50	10.00	21.70	17.20	24.60	20.80		13.00	
Mo	<2.00	<2.00	<2.00	<2.00	<2.00	<2.00	<2.00	<2.00	<2.00	<2.00	<2.00	<2.00	<2.00			<2.00	3.40
Ag	<0.50	<0.50	0.80	<0.50	<0.50	<0.50	<0.50	<0.50	<0.50	<0.50	<0.50	<0.50	<0.50			<0.50	
In	<0.10	<0.10	<0.10	<0.10	<0.10	<0.10	<0.10	<0.10	<0.10	<0.10	<0.10	<0.10	<0.10			<0.20	
Sn	10.00	10.0	15.0	11.0	7.00	11.00	10.00	5.00	8.00	6.00	8.00	7.00	12.00			4.00	
Sb	<0.20	<0.20	<0.20	<0.20	<0.20	<0.20	<0.20	<0.20	<0.20	<0.20	<0.20	<0.20	<0.20		<1.00	3.50	0.55
Cs	15.20	47.70	10.50	12.10	18.00	16.10	13.40	9.20	12.10	10.20	12.10	11.50	14.40	7.00	4.90	7.70	
Ba	146.00	591.00	563.00	593.00	697.00	530.00	620.00	557.00	506.00	577.00	457.00	481.00	339.00	721.00	268.00	494.00	
Hf	2.60	6.10	10.60	5.70	2.60	5.30	4.20	2.60	4.60	3.20	5.20	4.40	4.30	10.80	4.50	6.70	
Ta	1.95	4.10	2.20	1.60	2.32	2.45	1.87	1.17	2.58	1.05	2.82	2.21	2.69	4.76		1.20	
W	2.20	17.90	1.00	1.10	1.30	3.90	0.80	<0.50	1.60	1.20	2.90	2.20	2.00			2.00	

Table 1 *(continued)*

	Granite				Coarse-grained regolith			Fine-grained regolith					Bed sed.	Achala Batholith		Loess	
Sample	RM102	RM001A	RM109	RM110	RM108	RM001B	RM002B	RM005	RM006	RM008	RM009	RM010	RM007	ACH-135[1]	S5[2]	A[3]	C[4]
Tl	1.38	2.80	1.80	1.70	1.82	1.54	1.67	1.41	1.38	1.46	1.31	1.32	1.37			0.90	
Pb	27.00	36.00	42.00	41.00	44.00	38.00	44.00	38.00	33.00	39.00	31.00	32.00	29.00		29.00	31.00	
Bi	<0.10	4.60	<0.10	0.20	<0.10	0.50	0.30	0.50	1.50	0.20	1.10	1.20	0.60		<0.40	2.40	
Th	15.70	35.70	115.00	50.20	16.10	36.60	25.20	16.20	21.60	16.60	19.90	18.50	30.40	12.30	32.20	12.90	
U	4.87	4.00	4.00	3.10	1.89	3.56	3.06	2.25	3.69	2.48	3.44	3.20	3.95	5.05	2.60	3.20	3.00
La	27.00	35.00	147.00	74.50	30.20	60.50	51.50	27.70	41.00	28.80	37.20	34.20	47.30	45.00	38.65	34.30	
Ce	55.10	74.90	319.00	148.00	55.00	124.00	99.30	49.70	73.20	50.60	71.50	63.70	87.80	100.00	86.52	71.20	
Pr	6.27	8.50	37.80	17.80	6.81	14.20	11.40	6.21	8.97	6.54	8.12	7.33	10.70	12.70	8.82	7.80	
Nd	21.20	29.70	130.00	60.00	23.00	48.20	37.90	20.80	30.40	22.00	27.20	25.00	36.70	42.70	37.67	30.40	
Sm	3.98	5.80	19.80	9.90	4.06	8.67	6.59	3.60	5.36	3.80	4.81	4.27	6.26	8.61	7.13	6.10	
Eu	0.49	0.80	1.50	1.10	0.74	1.02	0.97	0.59	0.82	0.64	0.73	0.68	0.73	1.12	0.87	1.29	
Gd	2.54	4.20	8.80	5.40	2.63	5.27	4.24	2.02	3.56	2.25	3.17	2.87	3.65	6.65	4.34	5.40	
Tb	0.33	0.50	0.80	0.60	0.31	0.61	0.56	0.24	0.50	0.28	0.44	0.39	0.44	1.01	0.50	0.90	
Dy	1.69	2.60	3.30	2.60	1.45	2.64	2.59	1.03	2.43	1.32	2.27	1.96	1.98	5.26	1.99	5.20	
Ho	0.28	0.40	0.50	0.40	0.24	0.42	0.43	0.17	0.43	0.21	0.40	0.36	0.32	0.84	0.29	1.00	
Er	0.78	1.20	1.00	1.00	0.64	1.10	1.10	0.44	1.17	0.57	1.10	0.98	0.82	1.90	0.73	3.10	
Tm	0.11	0.18	0.10	0.13	0.09	0.15	0.15	0.06	0.17	0.08	0.17	0.14	0.11	0.22	0.11	0.48	
Yb	0.74	1.08	0.80	0.78	0.56	0.88	0.92	0.39	1.13	0.54	1.07	0.95	0.71	1.25	0.65	3.00	
Lu	0.11	0.15	0.10	0.12	0.08	0.13	0.13	0.06	0.17	0.08	0.17	0.14	0.11	0.19	0.08	0.45	
Eu/Eu^*_N	0.72**	0.74**	0.53**	0.68**	1.72	1.14	1.39	1.65	1.41	1.66	1.42	1.46	1.15				
Ce/Ce^*_N	4.10**	4.15**	4.12**	3.95**	0.90	0.99	0.96	0.89	0.89	0.86	0.96	0.93	0.91				
La/Yb_N	1.25**	1.11**	6.02**	3.28**	0.65	0.83	0.68	0.86	0.44	0.65	0.42	0.44	0.81				
CIW	65.9	74.7	68.1	69.6	72.9	68.5	69.3	71.4	70.3	70.9	70.3	70.5	65.6	66.7	69.2		
CIPW norm (%)																	
Qtz	39.51	32.78	29.18	28.20	29.99	28.83	25.56	39.94	38.8	36.15	36.86	39.02					
Kfs	23.43	37.07	33.51	35.34	40.89	32.51	38.14	33.52	26.6	33.69	26.87	27.87					
Pl	30.89	22.06	28.06	28.38	23.81	30.35	29.96	22.86	27.2	25.39	28.4	26.29					
Bt	2.70	3.12	5.38	4.44	1.95	4.26	3.33	1.56	3.15	1.93	3.36	3.01					
Ms	2.84	3.96	2.51	2.69	2.21	3.08	2.24	1.69	3.64	2.34	3.89	3.24					
Ap	0.42	0.65	0.73	0.53	0.44	0.55	0.46	0.26	0.2	0.31	0.2	0.22					

Total iron as Fe_2O_3.
$Eu/Eu^*_N = Eu / (Sm * Gd)^{0.5}$ (McLennan, 1989).
$Ce/Ce^*_N = Ce / (1/3Nd + 2/3La)$ (Elderfield et al., 1990).
N denotes normalization to average granite composition.
$CIW = 100[Al_2O_3 / (Al_2O_3 + CaO + Na_2O)]$ (Harnois, 1988).
[1] Coarse-grained porphyritic monzogranite of the Achala Batholith (Dahlquist et al., 2013).
[2] Monzogranite of the Achala Batholith (Piovano, personal communication).
[3] Loess from Ancasti (Catamarca Province).
[4] Mean value (n = 50) for loess from Córdoba Province (Nicolli et al., 1989).
** Granites normalized to UCC (McLennan, 2001).

Although total annual rainfall is significant, steep slopes and very thin and incipient soils, as well as shallow sediment accumulations, yield a scattered vegetation of grassland, varied shrubbery and the particularly widespread *Parkinsonia aculeate*.

3. Methods

3.1. Sampling

Representative samples of granite and regolith were collected in the spring of 2009. We use here the term "regolith" in the sense of Scott and Pain (2009), i.e., "…unconsolidated or secondarily re-cemented cover that overlies more coherent bedrock, and which has been formed by weathering, erosion, transport and/or deposition of the older material. According to this definition, regolith includes a set of materials, in situ or transported, such as fractured and weathered basement rocks, saprolites, alluvium, colluvium, soils, organic accumulations, glacial deposits, aeolian deposits, evaporitic sediments…". Three kinds of samples were collected (Table 1): a) unweathered granite (representative samples RM-001A, RM-102, RM-109 and RM-110, Fig. 1B); b) coarse-grained regolith, friable rock with texture still rather similar to the previous one but the sample can be "crumbled between one's fingers" (Middelburg et al., 1988), which has been transported for a relatively short distance from its source (samples RM-108, RM-001B and RM-002B; Fig. 1B); and c) alluvium (i.e., fine-grained regolith from a textural point of view), which is sediment that has accumulated within topographic depressions following relatively long distance transportation (samples RM-005, RM-006, RM-008, RM-009 and RM-010; Fig. 1B). One sample of river bed sediment, considered here as fine-grained regolith (sample RM-007; Fig. 1B) was also collected.

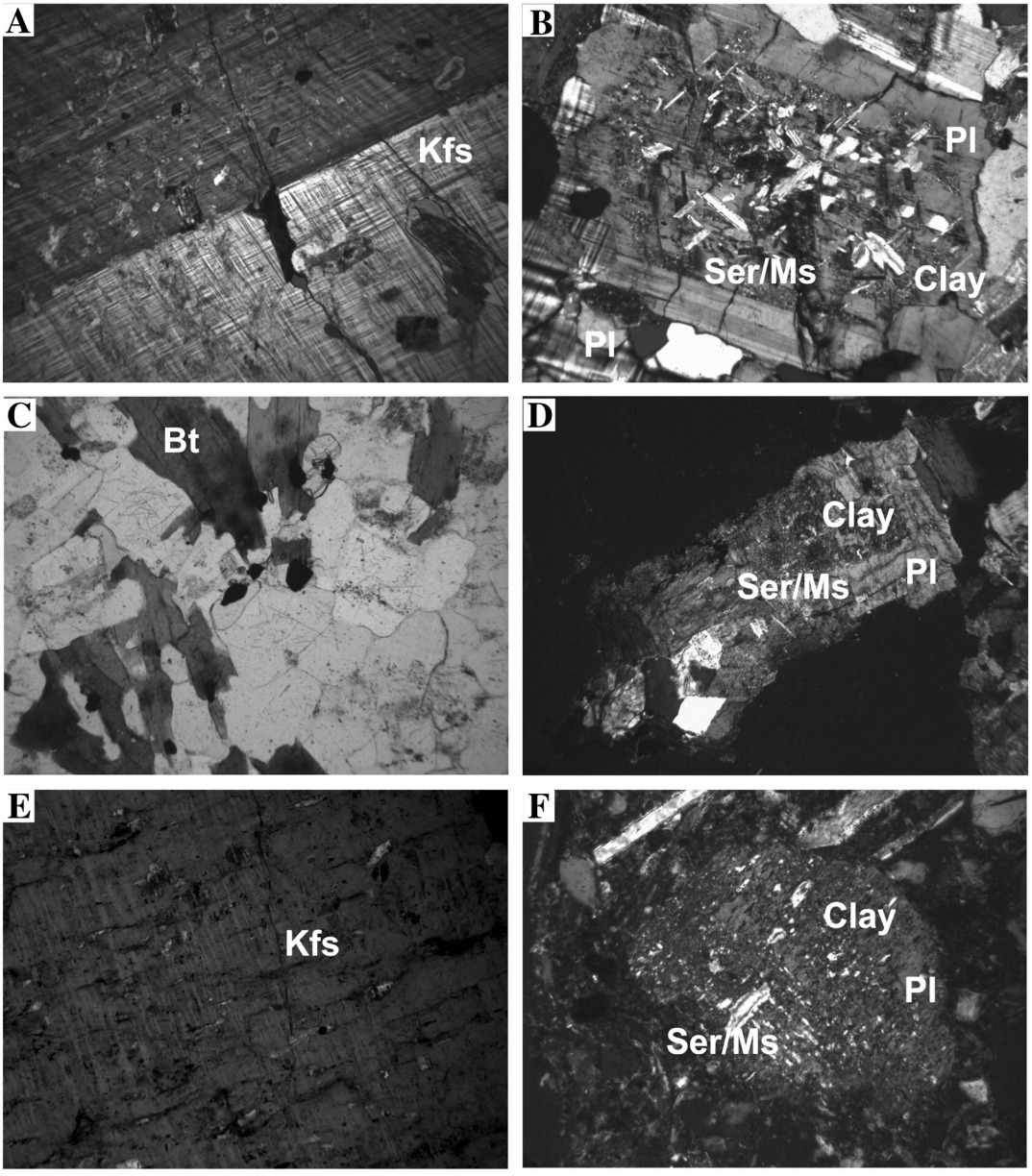

Fig. 3. Optical photomicrographs of the porphyritic monzogranite, and coarse- and fine-grained regolith samples. A) Perthitic K-feldspar (Kfs) in granite. B) Plagioclase (Pl) altered to sericite (Ser), secondary muscovite (Ms), and clay material in granite. C) Fe-oxide segregations on the crystal edges of biotite in granite. D) Plagioclase (Pl) altered to sericite (Ser), secondary muscovite (Ms), and clay minerals in the coarse-grained regolith. The alteration occurs primarily in the cores of zoned plagioclase crystals. E) Plagioclase (Pl) altered to sericite (Ser), secondary muscovite (Ms), and clay minerals in the fine-grained regolith. Plagioclase crystals are almost completely replaced by alteration products. F) Alteration on K-feldspar (Kfs) crystals along the plagioclase-rich domains of perthite in the fine-grained regolith. Width of photomicrographs: A) 7 mm; B) and C) 3 mm; D) and F) 6 mm; E) 1.5 mm.

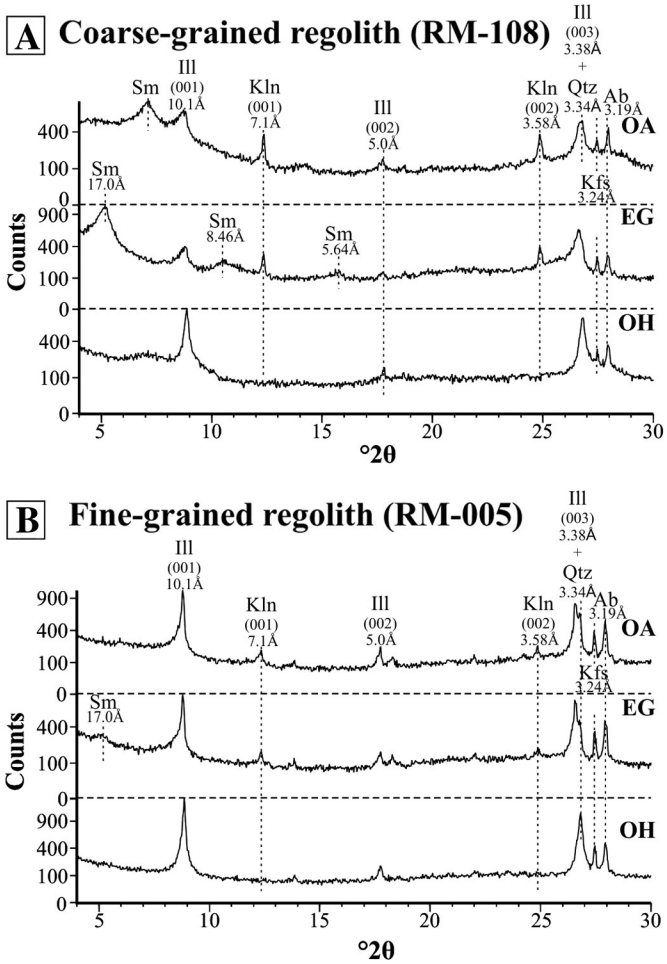

Fig. 4. X-ray diffractograms of the clay-size fractions (<2 μm) of: A) coarse-grained regolith (RM-108) and B) fine-grained regolith (RM-005). OA = oriented aggregates dried in air; EG = solvated in ethylene glycol; and OH = heated at 500 °C for 4 h. Ill = illite; Kln = kaolinite; Sm = smectite; Qtz = quartz; Ab = albite; Kfs = K-feldspar.

3.2. Petrological characterization and clay-size mineralogy

Thin section study of granite (n = 4), coarse-grained (n = 3), and fine-grained regolith samples (n = 5) was focused on characterization of mineral phases and textures. In as much as the traditional point count method is unsuitable for unconsolidated material, another method, such as the CIPW norm (Cross et al., 1902) was used to study country rock and regolith samples. This method converts the chemical composition of an igneous rock to an ideal mineral composition. Such an approach is justified because the resulting mineral percentages agree closely with the point counting mode in the granite country rock.

Samples for clay-mineral X-ray analysis were prepared following the recommendations of Moore and Reynolds (1997). The <2 μm size-fraction (representative of allochthonous dust, as well as autochthonous, neoformed, and transformed phases) from coarse- and fine-grained regoliths (n = 3) was analyzed in oriented aggregates dried in air (OA), ethylene-glycol solvated (EG) and heated at 500 °C (OH). X-ray analyses were performed with an X'Pert Pro diffractometer, using Cu Kα radiation, scanning from 4° to 30° 2θ with a step size of 0.03° 2θ and a scan time of 0.5 s per step. Illite (Ill) was identified by the presence of 10.1 Å (001), 5.0 Å (002) and 3.38 Å (003) reflections in the OA diagram, which showed no modifications in the EG and OH diagrams. The appearance of reflections at ~17.0, 8.46 and 5.64 Å in the EG diagram indicated the presence of expandable phases such as smectite (Sm). Reflections at 7.1 and 3.58 Å in the OA diagram, which disappeared in the OH diagram, revealed the presence of kaolinite (Kln). Residual quartz (3.34 Å reflection), K-feldspar (3.24 Å reflection), and albite (3.68 and 3.19 Å reflections) were also recognized in the <2 μm size-fraction.

3.3. Chemical analysis

Whole rock major and trace elements were determined in granite, coarse- and fine-grained regoliths using inductively coupled plasma (ICP, major elements) and inductively coupled plasma-mass spectrometry (ICP-MS, trace and rare earth elements). The analytical work was performed by Activation Laboratories Ltd. (ACTLABS, Ontario, Canada). Three blanks and five controls (three before the sample group and two after) were analyzed. Duplicates were fused and analyzed every 15 samples. The instrument was recalibrated every 40 samples.

3.4. Weathering assessment: geochemical and statistical tools

Weathering indices are useful to understand and evaluate element mobility during the chemical alteration of rocks. Several indices are defined in the literature (e.g., Depetris at al., 2014 and references therein); most of them compare the concentration of an immobile element with several mobile components. The Chemical Index of Weathering (CIW, Harnois, 1988) was calculated here to characterize the chemical alteration processes in the study area. The CIW (Eq. (1)) considers Al_2O_3 as the immobile component, while CaO and Na_2O are the mobile components because they are readily leached during weathering:

$$CIW = 100[Al_2O_3/(Al_2O_3 + CaO + Na_2O)]. \quad (1)$$

This index does not take into account potassium because it may be adsorbed on clays through ion exchange during chemical alteration (Harnois, 1988). In the studied area, CIW would produce more meaningful results because coarse-grained regolith samples appeared relatively enriched in K-feldspar. Therefore, the difference of CIW between source rock and sediment would reflect more precisely than other indices the extent of chemical weathering experienced by the weathered material. A one-way ANOVA and the non-parametric Kruskal–Wallis rank sum test (Davis, 1986) were performed in order to establish if there are significant differences among the CIW values calculated for granite (n = 4), coarse- (n = 3), and fine-grained regolith (n = 5) samples.

Geochemical datasets are multivariate and each sample has several major and trace elements (including REE). The main difficulty in assessing multi-element data is multi-dimensional visualization. A number of techniques can be used, including the multielement diagrams "spider diagrams" or "spidergrams", which plot values for a range of elements (connected by lines) in each sample (McQueen, 2009). Typically these plots involve normalizing the data to a reference sample. We produced spidergrams for major and trace elements in order to analyze the fractionation between the country rock and the regolith, using the average granite composition (n = 4) for normalization.

In order to test if the fractionation observed on the spidergrams (i.e., a qualitative approach) was statistically significant, the Woronow and Love (1990) log-ratio technique was used to calculate the mass changes that may have accompanied the conversion of granite to coarse- and fine-grained regoliths. For this purpose, the chosen element was one whose mass was conserved through the weathering process. The log-ratio Al_2O_3/Na_2O passed the 2-sample Kolmogorov–Smirnov test, the Mann–Whitney *U* test, the Ague (1994) bivariate plot, and the tests for subcompositional invariance and independence (e.g., Schedl, 1998; Woronow and Love, 1990). Hence, these two elements (i.e., Al and Na) have the statistical properties of immobility and their masses were likely conserved during weathering, mass wasting, and fluvial

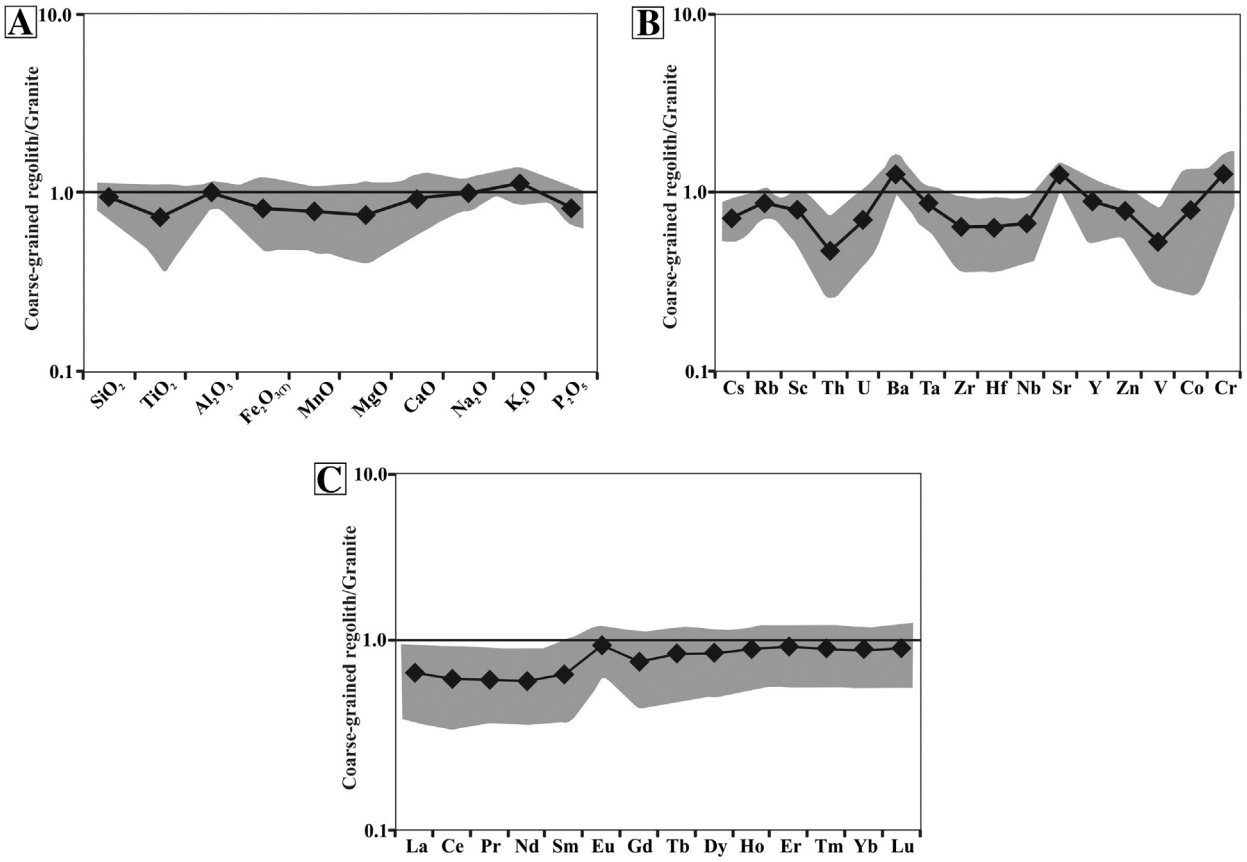

Fig. 5. Granite-normalized multielement diagrams of: A) major oxides, B) trace elements and C) REE, for coarse-grained regolith samples. Mean value is represented by thick line and standard deviation by the shaded area.

transportation. To facilitate the comparison with other weathering studies we present here the results using Al_2O_3 as the framework oxide.

Several ternary diagrams have been used for the analysis of the evolution of weathering (e.g., Nesbitt and Young, 1982, 1989). Through the Al_2O_3–($CaO^* + Na_2O$)–K_2O diagram (A–CN–K, where oxides are in molar proportion and CaO^* represents the CaO in the silicate fraction only) it is possible to plot the major rock composition, and the theoretical composition of several rock-forming minerals. The Al_2O_3–($CaO^* + Na_2O + K_2O$)–($FeO_{Total} + MgO$) diagram (A–CNK–FM) also includes ferromagnesian minerals (e.g., biotite). In the A–CN–K diagram, plagioclase (Pl) and K-feldspar (Kfs) plot at 50% Al_2O_3 and define the feldspar tie line. The clay mineral group, kaolinite (Kln), chlorite (Chl), and gibbsite (Gbs) plot at 100% Al_2O_3 (Nesbitt et al., 1996). We used here both, A–CN–K and A–CNK–FM diagrams, to analyze the weathering trend in the studied area.

4. Results and discussion

4.1. Characterization of the country rock: granite

The dominant facies of the Achala Batholith (Facies B) was recognized in the study area (Fig. 1A and B). It is a gray and moderately fractured porphyritic monzogranite that was emplaced into the high-grade metamorphic basement during the Late Devonian. Pegmatitic and aplitic intrusive bodies are distributed throughout the country rock.

The porphyritic monzogranite is holocrystalline and is mainly composed of quartz, K-feldspar, plagioclase, biotite, and white mica. It is characterized by large K-feldspar phenocrysts set in a medium to fine quartz–feldspar matrix. Apatite, zircon, rutile, and opaque phases occur as accessory minerals, while clay minerals, sericite, chlorite and muscovite are present as secondary minerals. The CIPW normative mineralogy is 32.4% quartz, 32.3% K-feldspar, 27.3% plagioclase, 4.0% biotite, 3.0% muscovite, and 0.6% apatite. K-feldspar phenocrysts (from 2 mm to >2 cm) are subhedral and perthitic (Fig. 3A), whereas in the matrix, K-feldspar crystals are smaller (from 0.1 to 2 mm) and anhedral. Myrmekitic globular shaped intergrowths of quartz in plagioclase are common along boundaries between plagioclase and K-feldspar. Plagioclase (from 0.1 to 3 mm) is euhedral to subhedral and often shows incipient to moderate alteration to clays, sericite, and secondary muscovite (Fig. 3B). Such alteration occurs primarily in the cores of zoned plagioclase crystals. Biotite (from 0.1 to 2.5 mm) is subhedral and slightly chloritized. It is also replaced by secondary muscovite. Fe-oxide segregations have developed on the crystal edges of some biotites (Fig. 3C). Secondary muscovite, which was identified replacing plagioclase and biotite, is present in small proportions and is a product of the hydrothermal alteration that affected the Achala Batholith on a regional scale. Chloritization of biotite is also an effect of the deuteric alteration. Román-Ross et al. (1998) recognized the same mineral assemblage and alteration phases in the dominant facies (i.e., Facies B) of the Achala Batholith.

Whole rock chemical analyses performed on four granite samples (RM-001A, RM-102, RM-109 and RM-110) are shown in Table 1, along with the Chemical Index of Weathering (CIW, Harnois, 1988). Other samples of the dominant facies of the Achala Batholith (Dahlquist et al., 2013; Piovano, personal communication) are also included for comparison (Table 1). The granite S5 Monzogranite (Piovano, personal

Table 2
Mass balance changes in major, trace and REE that granite undergoes when compared to coarse- and fine-grained regolith samples in La Trucha drainage basin. Bold numbers indicate a statistically significant change at the 95% confidence level.

	Coarse-grained regolith			Fine-grained regolith		
Parameter	Maximum	Minimum	Average change (%)	Maximum	Minimum	Average change (%)
SiO_2	9	−17	−5	25	−2	11
Al_2O_3	0	0	0	0	0	0
$Fe_2O_{3(T)}$	50	−57	−20	24	−51	−22
MnO	17	−56	−28	**−21**	**−54**	**−40**
MgO	42	−62	−27	**−7**	**−64**	**−42**
CaO	70	−49	−7	24	−53	−24
Na_2O	25	−21	−1	27	−15	4
K_2O	52	−18	12	29	−24	−1
TiO_2	67	−68	−27	54	−55	−17
P_2O_5	17	−43	−18	**−37**	**−69**	**−56**
LOI	53	−37	−2	258	7	96
Sc	9	−44	−22	75	−56	−12
V	58	−80	−44	50	−72	−35
Cr	122	−29	26	157	0	60
Co	122	−76	−27	40	−71	−36
Rb	27	−41	−13	2	−40	−22
Sr	62	−3	25	66	0	29
Y	37	−46	−14	28	−53	−22
Zr	78	−74	−32	49	−60	−23
Nb	11	−62	−35	7	−59	−34
Cs	152	−70	−13	76	−74	−32
Ba	291	−49	42	237	−47	34
Hf	70	−73	−33	42	−60	−25
Ta	76	−52	−8	64	−56	−15
Th	106	−85	−44	43	−84	−53
U	11	−59	−33	11	−41	−19
La	157	−77	−23	81	−78	−37
Ce	149	−80	−29	61	−81	−45
Pr	156	−80	−28	73	−80	−42
Nd	152	−80	−29	70	−81	−43
Sm	120	−76	−28	47	−78	−43
Eu	94	−53	−4	55	−57	−18
Gd	84	−66	−21	7	−65	−39
Tb	67	−56	−14	16	−55	−28
Dy	42	−51	−17	18	−54	−26
Ho	42	−47	−13	35	−50	−18
Er	35	−40	−10	42	−47	−13
Tm	56	−41	−4	72	−45	−3
Yb	29	−40	−12	64	−44	−4
Lu	32	−40	−11	77	−40	3
T (bulk mass)	2	−10	−4	**14**	**1**	**7**

communication) shows a similar CIW (69.2) compared to the granite samples of this study (average CIW = 69.6), while sample ACH-135 (Dahlquist et al., 2013) exhibits a lower CIW (66.7).

4.2. Mineralogy and chemical composition of the coarse-grained regolith

The coarse-grained regolith in the upper catchments is mainly the result of the synergistic action of mechanical weathering and incipient chemical attack, which assists in rock physical breakdown. The material thus released is subsequently transported, and therefore, subjected to sorting. Most mineral debris that is relatively near to its source, is similar to the country rock, with grain-size oscillating between very coarse sand (12 mesh or ~2 mm mean grain-size), and fine sand (120 mesh or ~0.15 mm mean grain-size) or silt (270 mesh or ~62 μm mean grain-size).

The mean CIPW normative mineralogy for all coarse-grained regolith samples is 28.1% quartz, 37.2% K-feldspar, 28.0% plagioclase, 3.1% biotite, 2.5% muscovite, and 0.5% apatite. Quartz (from 1 to 5 mm) remains abundant and it retains its resistate character. K-feldspar crystals (from 0.5 to 11 mm) and muscovite (from 0.1 to 1.5 mm) display no alteration. Plagioclase (from 0.1 to 1 mm) exhibits the same alteration as granite samples. Such alteration to clay minerals, sericite, and secondary muscovite occurs primarily in the cores of zoned plagioclase crystals (Fig. 3D). Similarly, biotite (from 0.2 to 2 mm) shows a slight alteration to chlorite and secondary muscovite. Fe-oxide segregations are also observed on the crystal edges of some biotites. As described for granite, small amounts of secondary muscovite in plagioclase and biotite, and chloritization in biotite reflect the original regional hydrothermal alteration of the batholith. The accessory phases, apatite, zircon, rutile, and opaque phases, occur only in association with biotite aggregates, and are not distinguished in the matrix as in granite samples.

The clay-size fraction in the coarse-grained regolith is mainly composed of, in order of decreasing abundance, illite, kaolinite, and smectite (Fig. 4A). These clays are associated with clay-sized residual quartz, K-feldspar, and albite. Illite and kaolinite are probably associated with the hydrothermal alteration that affected the Achala Batholith. Also, the physical breakdown of muscovite likely yielded illite. Thus, smectite, which is not well developed, is the only clay mineral clearly associated with the weathering of the Achala Batholith. The clay-size fraction is principally autochthonous and the result of hydrothermal alteration and weathering by-products, but some may be allochthonous and supplied as wind-blown dust. However, the amount of allochthonous material in the study area must be negligible, as the loess signal from Ancasti (Catamarca Province, Argentina) and from Córdoba Province, Argentina (n = 50; Nicolli et al., 1989) does not appear to affect significantly the regolith composition (Table 1).

The distribution of major oxides, trace elements and REE in coarse-grained regolith samples is shown in granite-normalized extended multielement diagrams (Fig. 5). According to this qualitative approach, the

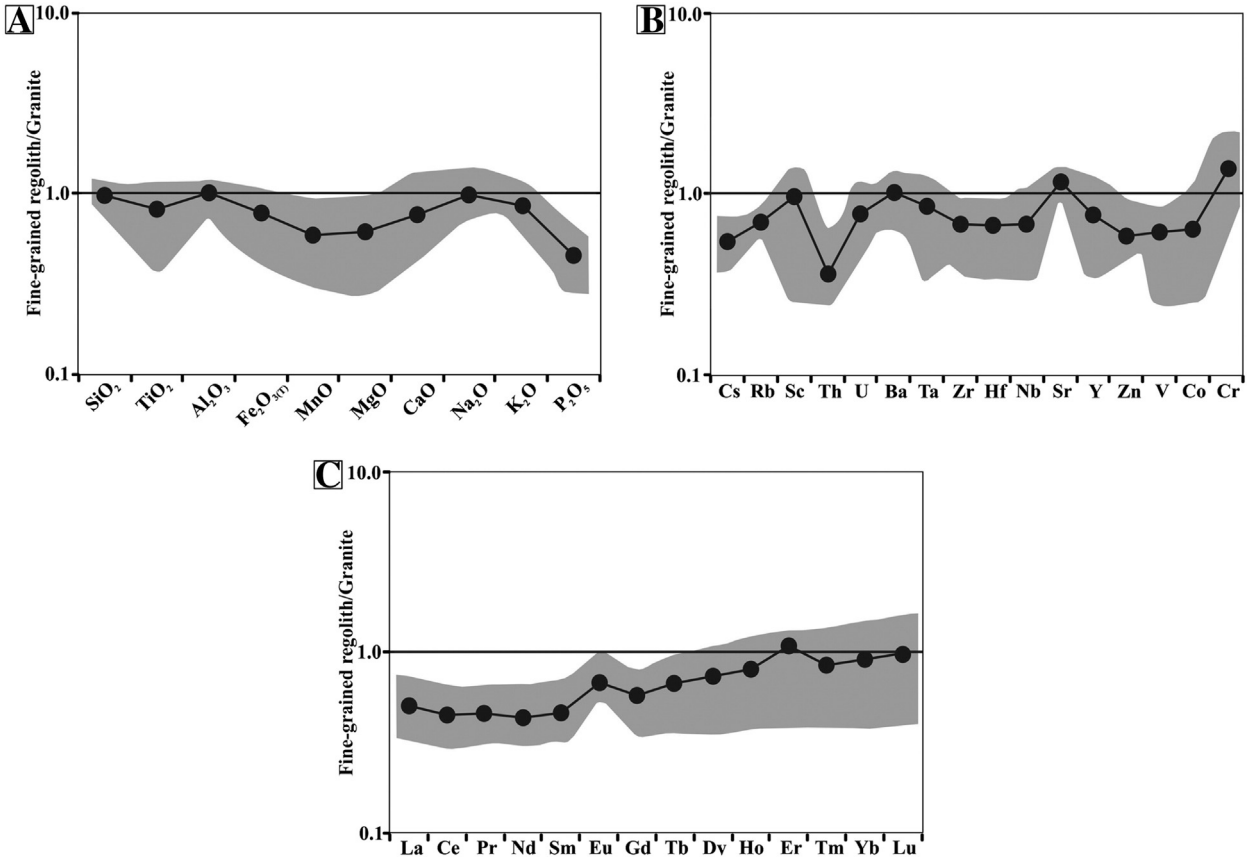

Fig. 6. Granite-normalized multielement diagrams of: A) major oxides, B) trace elements and C) REE, for fine-grained regolith samples. Mean value is represented by thick line and standard deviation by the shaded area.

coarse-grained regolith samples are slightly depleted in $Fe_2O_{3(T)}$, MnO, MgO, CaO, and P_2O_5 (Fig. 5A), as well as in most trace elements (i.e., Cs, Rb, Sc, Th, U, Ta, Zr, Hf, Nb, Y, Zn, V, and Co; Fig. 5B) and REE, with the light REEs (LREEs) exhibiting the largest depletion (Fig. 5C). Several studies have demonstrated that under some weathering conditions, REE are significantly mobilized and fractionated (e.g., Duddy, 1980; Gray, 2001; McQueen, 2006; Nesbitt, 1979; Sharma and Rajamani, 2000). In granitic rocks, the accessory minerals monazite, zircon and apatite have the higher REE concentrations, and the remaining REE content is present in other major mineral phases (i.e., biotite, feldspars, and mica) (e.g., Gromet and Silver, 1983).

The REE spidergram (Fig. 5C) shows slightly heavy REE-enriched (HREE) granite-normalized patterns, confirmed by the $(La/Yb)_N$ ratios (N denotes normalization to average granite composition), which range between 0.65 and 0.83 (Table 1). The Eu anomalies of coarse-grained regolith samples, normalized to average granite composition, vary between 1.14 and 1.72. The positive Eu/Eu* ratios can be attributed to the preferential retention of detrital feldspars in the coarse-grained size fraction compared to the original country rock. Nagasawa (1971) measured Eu anomalies in coexisting plagioclase and K-feldspar and concluded that Eu^{2+} was present in both feldspars and that it behaved very much like Sr^{2+}. Slightly negative Ce anomalies (Table 1) are also identified in the coarse-grained regoliths. Depletions of Ce in the coarse-size fraction likely reflect the alteration of apatite, a host mineral of the REEs, especially Ce (e.g., Banfield and Eggleton, 1989).

These depletions in major, trace elements and REE are likely associated with the alteration of biotite and apatite, as the CIPW norm suggests, and with the sorting of accessory minerals resistant to weathering, such as zircon, rutile, and monazite. On the other hand, the coarse-grained regolith samples are slightly enriched in K_2O (Fig. 5A), Ba, and Sr (Fig. 5B). These enrichments could be caused by the slightly larger relative abundance of detrital feldspar in the regolith than in the original country rock, as confirmed by the CIPW norm.

In order to test if the enrichments or depletions observed on the spidergrams (i.e., a qualitative approach, Fig. 5) are statistically significant, mass balance changes were calculated between the unweathered granite and the coarse-grained regolith. The obtained results (Table 2) indicate that the fractionation observed in the spidergrams is not statistically significant in any of the major, trace, or REE. Additionally, the change in bulk mass is not statistically significant (Table 2). Thus, no statistically significant chemical alteration or sorting effect appears to have affected the granite country rock during its conversion to coarse-grained regolith.

4.3. Mineralogy and chemical composition of the fine-grained regolith

Most fine-grained material is composed of fine sand (70 mesh or ~0.25 mm mean grain-size) and silt (270 mesh or ~62 μm mean grain-size) or clay (~2 μm mean grain-size).

The mean CIPW normative mineralogy for all fine-grained regolith samples is 38.1% quartz, 29.7% K-feldspar, 26.0% plagioclase, 2.6% biotite, 3.0% muscovite, and 0.2% apatite. Quartz (from 0.1 to 4 mm), due to its resistant character, and muscovite (from 0.1 to 1.5 mm) display no alteration. K-feldspar crystals (from 0.2 to 5 mm) show a slight alteration that affects the plagioclase-rich domains of perthite (Fig. 3E). Plagioclase (from 0.2 to 2 mm) exhibits a higher degree of alteration, which produces a dusty appearance under the microscope. Plagioclase crystals are almost completely replaced by clay minerals and sericite (Fig. 3F). Biotite (from 0.2 to 0.7 mm) in the fine-grained fraction shows a more intense segregation of Fe-oxides. Hydrothermal alteration products (i.e., secondary muscovite in plagioclase and biotite, and chlorite in biotite) are also observed in low proportions. The

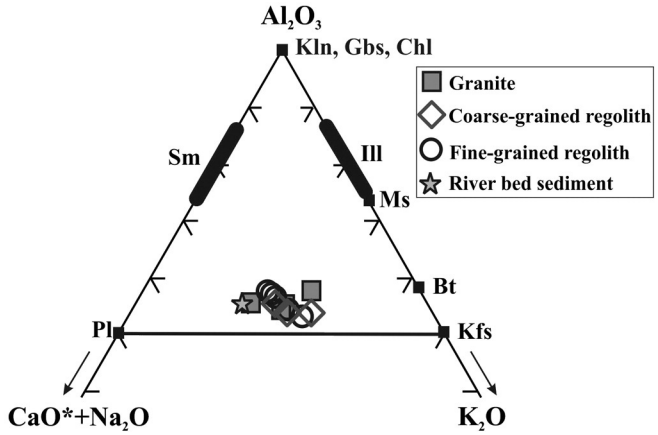

Fig. 7. Centered A–CN–K ternary plot (e.g., von Eynatten et al., 2002) for the analyzed samples (granite, coarse- and fine-grained regoliths). Oxides are in molar proportions and CaO* represents the CaO in the silicate fraction only (e.g., Nesbitt and Young, 1982, 1989). For this study CaO* was corrected for apatite. Kln = kaolinite; Gbs = gibbsite; Chl = chlorite; Sm = smectite; Ill = illite; Pl = plagioclase; Kfs = K-feldspar; Ms = muscovite; Bt = biotite.

accessory minerals apatite, zircon, rutile, and opaque phases are mostly inclusions in biotite. Argillaceous detritus was also observed in the matrix.

The <2 μm size-fraction was analyzed in sediment samples (RM-005 and RM-008) by means of X-ray diffraction. This fraction is composed of illite > kaolinite > smectite, and residual albite, K-feldspar, and quartz (Fig. 4B).

The distribution of major oxides, trace elements and REE in sediments that accumulated in topographic lows (samples RM-005, RM-006, RM-008, RM-009 and RM-010) and in the river bed (i.e., sample RM-007) is shown in the granite-normalized spidergrams (Fig. 6). As expected, the fine-grained regolith samples (alluvium) exhibit granite-normalized patterns similar to the coarse-size fraction, but are somewhat more depleted in soluble elements (Fig. 6A). The fine-grained regolith samples are depleted in $Fe_2O_{3(T)}$, MgO, MnO, CaO, P_2O_5, and K_2O (Fig. 6A), as well as in trace elements (i.e., Cs, Rb, Sc, Th, U, Ta, Zr, Hf, Nb, Y, Zn, V, and Co; Fig. 6B) and REE (Fig. 6C), especially in LREE, which appear more mobile compared to the granite country rock. These depletions could be associated with the alteration of biotite, plagioclase, K-feldspar, and apatite, and the effects of sorting on accessory phases resistant to weathering (i.e., rutile, monazite, and zircon). On the other hand, these sediments display a slight enrichment of Sr and Cr, both of which are likely adsorbed onto clays and Fe and Al oxyhydroxides (e.g., Middelburg et al., 1988).

The fine-grained regolith samples are more REE fractionated than the coarse-size fraction and the $(La/Yb)_N$ ratios range between 0.42 and 0.86 (Table 1). Positive Eu anomalies were also calculated in the fine-grained regolith samples. According to these ratios three groups of samples can be identified, which, as it will be seen in Figs. 8 and 9, seem to be connected with the degree of alteration reached by feldspar grains. The sediment samples located closer to the headwaters of the basin (RM-005 and RM-008) exhibit the higher Eu/Eu* ratios (average value 1.66), whereas the samples taken downstream (RM-006, RM-009, and RM-010) show Eu/Eu* ratios of about 1.43. Finally, the lowest Eu anomaly was estimated in the river bed sediment sample (RM-007, Eu/Eu* = 1.15). Negative Ce anomalies (average value 0.90) were also calculated in the fine-grained regolith samples. These Ce anomalies are likely the result of the alteration of apatite (e.g., Banfield and Eggleton, 1989).

Table 3
One-way ANOVA of the CIW of granite country rock, coarse- and fine-grained regolith samples of La Trucha drainage basin. The null hypothesis cannot be rejected at the 95% confidence level.

Source of variation	Sum of squares	df	Mean square	F	Significance level
Between groups	2.718	2	1.359	0.227	0.801
Within groups	53.822	9	5.980		
Total	56.540	11			

Table 4
ANOVA for the multiple linear model that describes the relationship of the Na/K and Ca/K ratios in granite, coarse- and fine-grained regolith samples.

Source of variation	Sum of squares	df	Mean square	F	Significance level
Na/K	0.0156	1	0.0156	21.500	0.004
Material	0.0066	2	0.0033	4.541	0.063
Na/K:Material	0.0007	2	0.0004	0.495	0.633*
Residuals	0.0044	6	0.0007		

* There are no significant differences between the slopes of the regressions for granite, coarse- and fine-grained regoliths.

As in the case of coarse-grained regolith, Table 2 also shows the mass balance changes between the granite and the fine-grained regolith. In this case, statistically significant changes at the 95% confidence level are determined for MgO, MnO, P_2O_5, and LOI in the sediment samples when compared to the country rock. Specifically, the masses of MgO, MnO and P_2O_5 were reduced in the fine-grained regolith by 42% (+35%/−22%), 40% (+19%/−14%), and 56% (+19%/−13%) respectively, while the masses of the volatiles included in the LOI parameter, increased by 96% (+162%/−89%). The significant depletions in these major oxides would be associated with incipient weathering that affected mainly apatite and biotite. On the other hand, the statistically significant increase in LOI mass can be translated into a nominally statistically significant increase in bulk mass.

4.4. The overview of weathering

A–CN–K and A–CNK–FM ternary diagrams are useful to assess the evolution of weathering in a drainage basin. Fig. 7 shows in an A–CN–

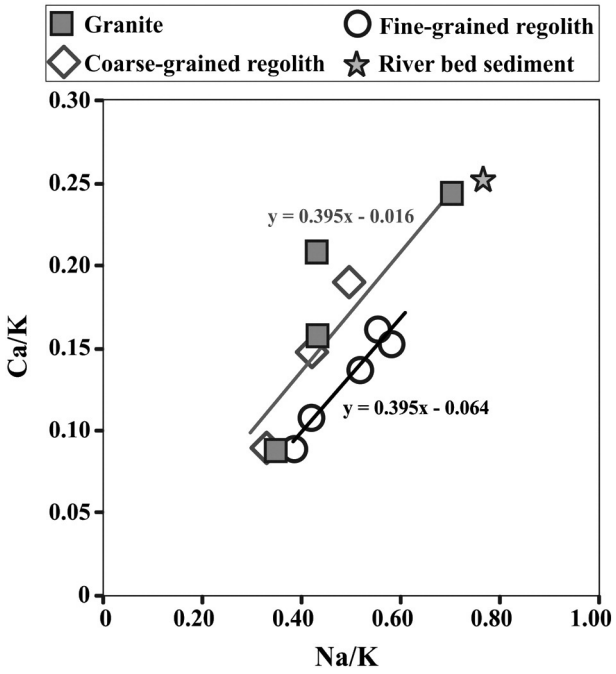

Fig. 8. Ca/K vs. Na/K plot for the coarse- and fine-grained regoliths, river bed sediment and granite. The upper line corresponds to granite and coarse-grained regolith; the lower one to fine-grained regolith. Both ratios rapidly diminish during the initial stages of weathering as a result of the greater alteration rate of plagioclase compared to K-feldspar (e.g., Nesbitt et al., 1980).

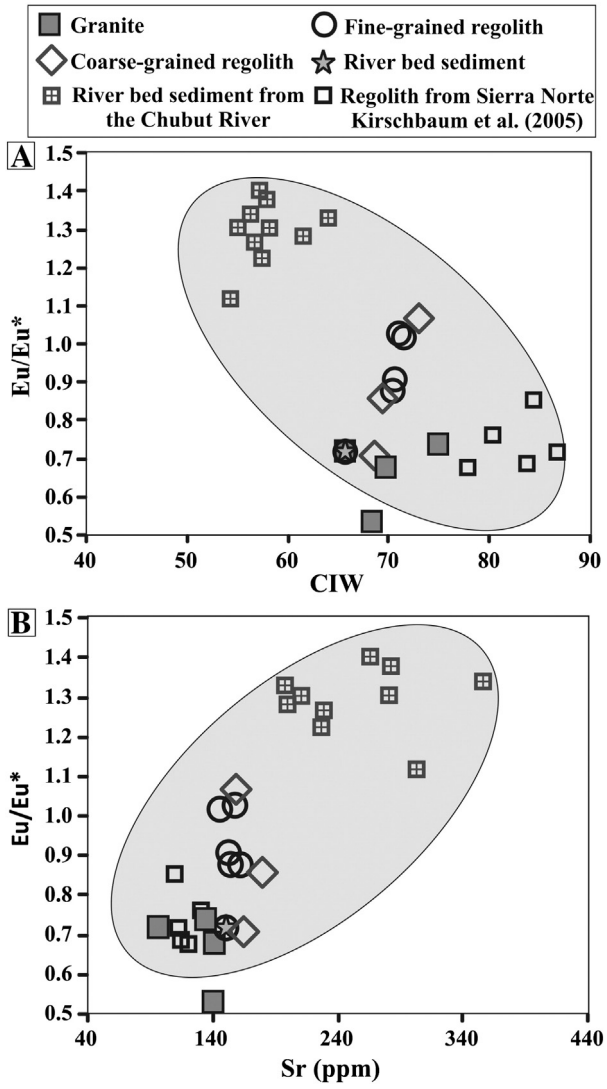

Fig. 9. A) Eu/Eu* vs. CIW and B) Eu/Eu* vs. Sr for the regolith and granite samples of the study area, regolith of the Sierra Norte (Kirschbaum et al., 2005), and river bed sediment of the Chubut River (Pasquini et al., 2005). $Eu/Eu^*_N = Eu/(Sm * Gd)^{0.5}$ (McLennan, 1989), where the subscript "N" denotes UCC-normalized values.

K plot, the granite country rock, and coarse- and fine-grained regoliths. All samples plot close to the feldspar tie line, indicating that feldspars are the dominant Al-bearing minerals in the granite, coarse- and fine-grained regoliths, as is also indicated by the CIPW norm. Further, the coarse- and fine-grained regolith samples cluster within the compositional field defined by the four granite samples, thus suggesting that the masses of Al_2O_3, CaO, Na_2O and K_2O were not significantly altered during weathering and transportation into or within La Trucha basin. Following the line of reasoning of Nesbitt et al. (1996), it is possible that the coarse- and fine-grained regoliths correspond to a coarse residue of erosion and sorting (comparatively enriched in feldspars and quartz), while the mud-fraction with a high concentration of clay minerals has been removed from the drainage basin. The river bed sediment sample (RM-007) plots closer to the CN boundary (contains more CaO + Na_2O relative to K_2O) when compared to the granite country rock. Consequently, it is likely that sample RM-007 contains relatively more fine-grained plagioclase than its source. In the A–CNK–FM ternary diagram (not shown), the coarse- and fine-grained regolith samples (i.e., including the river bed sediment sample) also cluster tightly within the compositional field defined by the four granite samples.

The CIW obtained for both, the coarse- and fine-grained regolith samples (means of 70.5 and 70.7, respectively, Table 1), are slightly higher than the one estimated for the granite country rock (mean of 69.6, Table 1). To test if these differences are statistically significant we ran a one way-ANOVA (Table 3). The results indicate that the null hypothesis (which states that there are no differences across the group of means of CIW for granite, coarse- and fine-grained regolith samples) cannot be rejected at the 95% confidence level. Hence, there are no significant differences between the unweathered granite and the regolith samples. We also ran a non-parametric Kruskal–Wallis rank sum test to compare the medians, and we obtained similar conclusions (Kruskal–Wallis chi-squared = 1.6211, p value = 0.4446). Thus, through the analysis of CIW variability it is possible to affirm that no significant alteration of the granite country rock occurs during weathering and transportation within the fluvial regime of La Trucha basin.

Na/K and Ca/K elemental ratios are also useful to evaluate the degree of chemical alteration because they rapidly decrease during the initial stages of weathering as a result of the greater alteration rate of plagioclase when compared to K-feldspar (e.g., Nesbitt et al., 1980). To test if there are significant differences between the relationship of the ratios Na/K and Ca/K in the unweathered granite, coarse- and fine-grained regoliths, we compared these ratios through a multiple linear model and its corresponding ANOVA. The obtained results (Table 4) show that there are not significant differences between the slopes of the three regressions, i.e., the angular coefficient is the same for all of

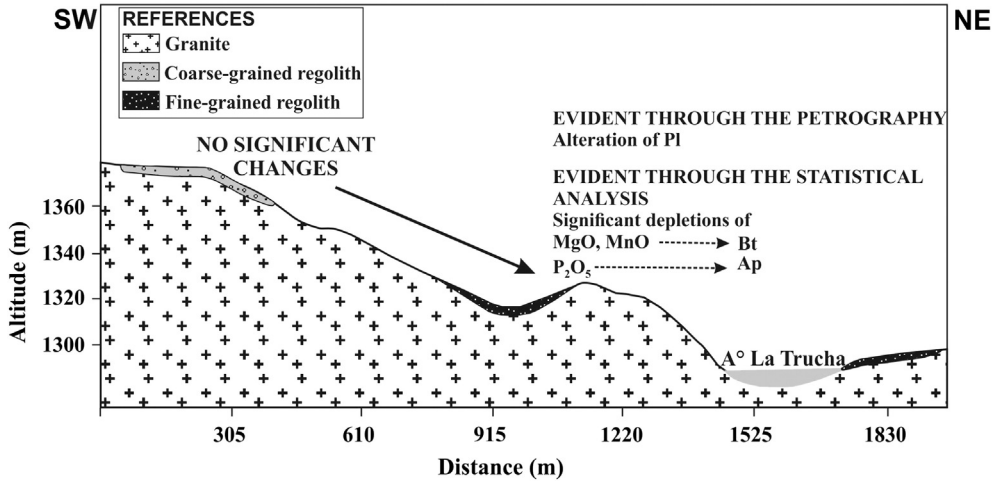

Fig. 10. Schematic section of the studied drainage basin, showing the mineralogical and statistically significant geochemical changes that occur in the coarse- and fine-grained regolith samples when compared to the granite country rock. Mineral abbreviations are after Kretz (1983). Pl = plagioclase; Bt = biotite; Ap = apatite.

them (F test = 0.495, p value = 0.633). We next ran a multiple linear model that explains the expected values of Ca/K for the three materials as a function of the Na/K values. The obtained results indicate that granite and coarse-grained regolith are not statistically different (Wald test = 0.376, p value: 0.717), whereas significant differences at the 90% confidence level were found between granite and fine-grained regolith (Wald test = −2.264, p value: 0.053). Finally, we ran a new multiple linear model to explain the analyzed relationship (i.e., Na/K and Ca/K), considering that granite and coarse-grained regolith are similar among them, whereas both are different when compared to the fine-grained regolith. Two linear regressions were obtained as a result of the model (Fig. 8). The significance of the regression parameter related to the type of material was also tested by means of an ANOVA (F value: 11.335; p value: 0.008). Therefore, these results are consistent with those obtained through the mass balance changes, indicating that several chemical differences are recorded between granite and fine-grained regolith, whereas the coarse-grained regolith samples do not show significant losses or gains of mass with respect to granite.

Fig. 9A illustrates the relationship between Eu anomaly (Eu/Eu*, normalized to the UCC, McLennan, 2001) and CIW for the samples of this study, including for comparison regolith samples of Sierra Norte (Kirschbaum et al., 2005) and river bed sediments of the Chubut River (Pasquini et al., 2005). Gao and Wedepohl (1995) found for Archean pelites a negative correlation between both parameters. Although a negative trend is observed for all the samples plotted, the regolith samples of the study area show what appears to be a positive correlation probably due to the effect of sorting and the relative proportion of minerals that contain Eu (mainly feldspars). The negative Eu/Eu*–CIW correlation is accompanied by a positive Eu/Eu*–Sr correlation for all samples (Fig. 9B). This correlation indicates the close relationship between Eu and Sr, which mainly substitute for Ca^{2+} in plagioclase and K^{+} in K-feldspar (Scott and Pain, 2009).

Fig. 10 shows a schematic section of the studied drainage basin with the mineralogical and statistically significant geochemical changes that occur in the coarse- and fine-grained regolith samples when compared to the country rock. The coarse-grained regolith samples do not exhibit statistically significant mass changes when compared to granite. On the other hand, in the fine-grained regolith samples, chemical attack is evident through the alteration of plagioclase, which was recognized in the analyzed thin sections, and the statistically significant loss of MgO, MnO, and P_2O_5, which is likely attributable to the alteration of biotite and apatite.

5. Conclusions

La Trucha is a small drainage basin that is representative of hundreds of first and second order streams that constitute the upper catchments of the fluvial system that dissects the Achala Batholith, in central Argentina. This is an intrusive acid body of Devonian age that occupies about 2500 km^2 in the uppermost region of the Sierra de Comechingones and Sierra Grande. The landscape is typical of a denuded scenario, but our current investigation shows that it is an example of a classical weathering-limited regime with little to no chemical denudation. Thus, the landscape is a relict of conditions prevailing during Carboniferous Gondwana times (Carignano et al., 1999). In as much as weathering occurs at a slower rate than erosion, there are no soil profiles that would assist in the assessment of weathering intensity.

Mechanical weathering appears to play a significant role in rock breakdown. The result is a relatively thin-layered regolith distributed all over the drainage basin. Therefore, there is a coarse-grained regolith that is characterized by a slightly larger relative abundance of detrital feldspar than the unweathered country rock (granite), and a fine-grained regolith, considerably finer than the first one, that accumulated in topographic depressions (i.e., in floodplain settings). Petrographic analyses show that plagioclase exhibits the same alteration in granite and coarse-grained regolith, which occurs primarily in the cores of zoned plagioclase crystals. Some Fe-oxide segregations that develop on the crystal edges of biotites are also recognized in both, coarse- and fine-grained regoliths. In the fine-grained regolith, plagioclase occurs in smaller proportions than in the country rock and is almost completely replaced by clay minerals and sericite. K-feldspar shows a slight alteration that affects the plagioclase-rich domains of perthite.

Chemical mass balance calculations performed between unweathered granite and both, coarse- and fine-grained regoliths, indicate that in the coarser fraction there are no statistically significant chemical changes in any of the major, trace, or REE. Furthermore, statistically significant losses of MgO, MnO, and P_2O_5 within the fine-grained regolith are attributable to incipient alteration of biotite and apatite. The mean CIW for coarse- and fine-grained regolith samples are slightly higher than the one estimated for the granite country rock; however, statistical analyses indicate that there are no significant differences in the CIW among unweathered granite and regoliths. The results of the multiple linear model and the corresponding ANOVA analysis of the relationship between the Na/K and Ca/K ratios in the granite country rock, coarse- and fine-grained regoliths are consistent with those obtained through the analysis of mass balance changes, indicating that several chemical differences are recorded between granite and fine-grained regolith, whereas the coarse-grained regolith samples do not show significant changes with respect to the country rock.

In the A–CN–K ternary diagram, the coarse- and fine-grained regolith samples cluster within the compositional field defined by the unweathered granite, thus suggesting that there are no significant losses of Al_2O_3, CaO, Na_2O and K_2O in the regolith when compared to the country rock. Apparently, the regolith corresponds to a coarse residue comparatively enriched in feldspars (and quartz). Such a conclusion implies that the mud-fraction with a high concentration of clay minerals has been removed from the high-energy drainage basin. All of the above results clearly indicate that there is little or no chemical alteration of the granite country rock during weathering and transportation within the fluvial La Trucha drainage basin.

This study performed in a pilot area of the highest ranges of the Sierra de Comechingones allowed the assessment of the effects of a dominant weathering-limited erosional setting that projects an image of mechanical weathering operating in synergy with little chemical attack. Such alteration is recorded in the fine-grained regolith that accumulated in topographic depressions, and it mainly affects plagioclase (evident through petrographical observations), biotite, and apatite (indicated by the statistical analysis of its chemistry).

Acknowledgments

This research was funded by the Universidad Nacional de Córdoba, Argentina (SECYT) and by Argentina's Consejo Nacional de Investigaciones Científicas y Técnicas (CONICET). We thank Dr. Edgardo Baldo for his support with the petrographic characterization and CIPW norm calculation. We also thank Dr. Viviana Giampaoli for her assistance in the statistical analyses. We would also like to thank an anonymous reviewer whose constructive suggestions helped to significantly improve this work.

References

Ague, J.J., 1994. Mass transfer during Barrovian metamorphism of pelites, south-central Connecticut. I: Evidence for changes in composition and volume. Am. J. Sci. 294, 989–1057.

Banfield, J.F., Eggleton, R.A., 1989. Apatite replacement and rare earth mobilization, fractionation, and fixation during weathering. Clay Clay Miner. 37 (2), 113–127.

Berner, R.A., 1992. Weathering, plants and the long-term carbon cycle. Geochim. Cosmochim. Acta 56, 3225–3231.

Berner, R.A., Lasaga, A.C., Garrels, R.M., 1983. The carbonate–silicate geochemical cycle and its effect on atmospheric carbon dioxide over the past 100 million years. Am. J. Sci. 283, 641–683.

Bonalumi, A., Martino, R.D., Sfragulla, J., Baldo, E.G., Zarco, J., Carignano, C.A., Tauber, A., Kraemer, P., Escayola, M., Cabanillas, A., Juri, E., Torres, B., 1998. Hoja geológica 3166-IV, 1:250,000, Villa Dolores. BulletinInstituto de Geología y Recursos Minerales, SEGEMAR, Argentina, p. 250.
Capitanelli, R.G., 1979. Geomorfología. In: Vasquez, J.B., Miatello, R., Roqué, M.E. (Eds.), Geografía Física de la Provincia de Córdoba. Boldt, Córdoba, pp. 213–296.
Carignano, C.A., Cioccale, M.A., Rabassa, J., 1999. Landscape antiquity of the central-eastern Sierras Pampeanas (Argentina): geomorphological evolution since Gondwanic times. Z. Geomorphol. Ann. Geomorph. 118 (Suppl.-Bd), 245–268.
Carson, M.A., Kirkby, M.J., 1972. Hillslope Form and Processes. Cambridge University Press, Cambridge (476 pp.).
Cross, W., Iddings, J.P., Pirsson, L.V., Washington, H.S., 1902. A quantitative chemico-mineralogical classification and nomenclature of igneous rocks. J. Geol. 10 (6), 555–690.
Dahlquist, J.A., Alasino, P.H., Bello, C., 2013. Devonian F-rich peraluminous A-type magmatism in the proto-Andean foreland (Sierras Pampeanas, Argentina): geochemical constraints and petrogenesis from the western-central region of the Achala Batholith. Mineral. Petrol. http://dx.doi.org/10.1007/s00710-013-0308-0.
Davis, J.C., 1986. Statistics and Data Analysis in Geology, 2nd ed. John Wiley and Sons, Singapore (646 pp.).
Demange, M., Alverez, J.O., Lopez, L., Zarco, J.J., 1996. The Achala Batholith (Cordoba, Argentina): a composite intrusión made of five independent magmatic suites. Magmatic evolution and deuteric alteration. J. S. Am. Earth Sci. 9, 11–25.
Depetris, P.J., Pasquini, A.I., Lecomte, K.L., 2014. Weathering and the Riverine Denudation of Continents. Springer Briefs in Earth System Sciences. Springer, Berlin 978-94-007-7716-3.
Dorais, M.J., Lira, R., Chen, Y., Tingey, D., 1997. Origin of biotite–apatite-rich enclaves, Achala Batholith, Argentina. Contrib. Mineral. Petrol. 130, 31–46.
Duddy, I.R., 1980. Redistribution and fractionation of rare-earth elements and other elements in a weathering profile. Chem. Geol. 30, 363–381.
Elderfield, H.R., Upstill-Goddard, R., Sholkovitz, E.R., 1990. The rare earth elements in rivers, estuaries and coastal sea waters: processes affecting crustal input of elements to the ocean and their significance to the composition of sea water. Geochim. Cosmochim. Acta 54, 971–991.
Gao, S., Wedepohl, K.H., 1995. The negative Eu anomaly in Archean sedimentary rocks: implications for decomposition, age and importance of their granitic sources. Earth Planet. Sci. Lett. 133, 81–94.
González Bonorino, F., 1950. Algunos problemas geológicos de Sierras Pampeanas. Rev. Assoc. Geol. Argent. 5 (3), 81–110.
Gordillo, C.E., 1984. Migmatitas cordieríticas de las Sierras de Córdoba; condiciones físicas de la migmatización. 68. Ac. Nac. de Ciencias de Córdoba, Miscelánea, pp. 1–40.
Gray, D.J., 2001. Hydrogeochemistry in the Yilgarn Craton. Geochem. Explor. Environ. Anal. 1, 253–264.
Gromet, L.P., Silver, L.T., 1983. Rare earth element distributions among minerals in a granodiorite and their petrogenetic implications. Geochim. Cosmochim. Acta 47, 925–939.
Hall, K., Thorn, C., Sumner, P., 2012. On the persistence of weathering. Geomorphology 149–150, 1–10.
Harnois, L., 1988. The CIW index: a new Chemical Index of Weathering. Sediment. Geol. 55, 319–322.
Isacks, B.L., 1988. Uplift of the Central Andean Plateau and bending of the Bolivian orocline. J. Geophys. Res. 93 (B4), 3211–3231.
Jordan, T., Allmendinger, R., 1986. The Sierras Pampeanas of Argentina; a modern analogue of the Rocky Mountain foreland deformation. Am. J. Sci. 286, 737–764.
Kirschbaum, A.M., Martinez, E., Pettinari, G., Herrero, S., 2005. Weathering profiles in granites, Sierra Norte (Córdoba, Argentina). J. S. Am. Earth Sci. 19, 479–493.
Krauskopf, K.B., Bird, D.K., 1995. Introduction to Geochemistry, 3rd ed. McGraw-Hill International Editions, New York (647 pp.).
Kretz, R., 1983. Symbols for rock-forming minerals. Am. Mineral. 68, 277–279.
Lira, R., Kirschbaum, A.M., 1990. Geochemical evolution of granites from the Achala Batholith of the Sierras Pampeanas, Argentina. Geol. Soc. Am. Spec. Pap. 241, 67–76.
Lobens, S., Bense, F.A., Wemmer, K., Dunkl, I., Costa, C.H., Layer, P., Siegesmund, S., 2011. Exhumation and uplift of the Sierras Pampeanas: preliminary implications from K–Ar fault gouge dating and low-T thermochronology in the Sierra de Comechingones (Argentina). Int. J. Earth Sci. 110 (2–3), 671–694.
McLennan, S.M., 1989. Rare earth elements in sedimentary rocks: influence of provenance and sedimentary processes. In: Lipin, B.P., McKay, G.A. (Eds.), Geochemistry and Mineralogy of Rare Earth Elements. Mineralogical Society of America, pp. 169–200.
McLennan, S.M., 2001. Relationships between the trace element composition of sedimentary rocks and upper continental crust. Geochem. Geophys. Geosyst. 2 (2000GC000109).
McQueen, K.G., 2006. Unravelling the regolith with geochemistry. In: Fitzpatrick, R., Shand, P. (Eds.), Regolith 2006 — Consolidation and Dispersion of Ideas. CRC LEME, Perth, pp. 230–235.
McQueen, K.G., 2009. Regolith geochemistry. In: Scott, K.M., Pain, C.F. (Eds.), Regolith Science. Springer-CSIRO Publishing, Dordrecht-Melbourne, pp. 73–104.
Middelburg, J.J., van der Weijden, C.H., Woittiez, J.R., 1988. Chemical processes affecting the mobility of major, minor and trace elements during weathering of granitic rocks. Chem. Geol. 68, 253–273.
Moore, D.M., Reynolds, R.C., 1997. X-ray Diffraction and the Identification and Analysis of Clay Minerals. Oxford University Press, New York (378 pp.).
Nagasawa, H., 1971. Partitioning of Eu and Sr between coexisting plagioclase and K-feldspar. Earth Planet. Sci. Lett. 13, 139–144.
Nesbitt, H.W., 1979. Mobility and fractionation of rare earth elements during weathering of a granodiorite. Nature 279, 206–210.
Nesbitt, H.W., Young, G.M., 1982. Early Proterozoic climates and plate motions inferred from major element chemistry of lutites. Nature 199, 715–717.
Nesbitt, H.W., Young, G.M., 1989. Formation and diagenesis of weathering profiles. J. Geol. 97, 129–147.
Nesbitt, H.W., Markovics, G., Price, R.C., 1980. Chemical processes affecting alkalis and alkaline earths during continental weathering. Geochim. Cosmochim. Acta 44, 1659–1666.
Nesbitt, H.W., Young, G.M., McLennan, S.M., Keays, R.R., 1996. Effects of chemical weathering and sorting on the petrogenesis of siliciclastic sediments, with implications for provenance studies. J. Geol. 104, 525–542.
Nicolli, H., Suriano, J., Gómez Peral, M., Ferpozzi, O., Baleani, O., 1989. Groundwater contamination with arsenic and other trace elements in an area of the Pampa, Province of Córdoba, Argentina. Environ. Geol. Water Sci. 14, 3–16.
Otamendi, J.E., Patiño Douce, A.E., Demichelis, A.H., 1999. Amphibolite to granulite transition in aluminous greywackes from the Sierra de Comechingones, Argentina. J. Metamorph. Geol. 17, 415–434.
Pasquini, A.I., Depetris, P.J., Gaiero, D.J., Probst, J.-L., 2005. Material sources, chemical weathering and physical denudation in the Chubut River basin (Patagonia, Argentina): implications for Andean Rivers. J. Geol. 113, 451–469.
Pasquini, A.I., Lecomte, K.L., Piovano, E.L., Depetris, P.J., 2006. Recent rainfall and runoff variability in central Argentina. Quat. Int. 158, 127–139.
Pinotti, L.P., Coniglio, J.E., Esparza, A.M., D'Eramo, F.J., Llambías, E.J., 2002. Nearly circular plutons emplaced by stoping at shallow crustal levels, Cerro Áspero batholith, Sierras Pampenas de Córdoba, Argentina. J. S. Am. Earth Sci. 15, 251–265.
Pope, G.A., 2013. Weathering and sediment genesis. In: Shroeder, J., Pope, G. (Eds.), Treatise on Geomorphology. Academic Press, San Diego, pp. 284–293.
Rabassa, J., Zárate, M., Cioccale, M.A., Carignano, C.A., Partridge, T., Maud, R., 1996. Paisajes relictuales de edad gondwánica en areas cratónicas de Argentina. Actas 13° Congreso Geológico Argentino y 3° Congreso de Exploración de Hidrocarburos. 4, p. 219 (Buenos Aires, Argentina).
Rapela, C.W., Pankhurst, R.J., Casquet, C., Baldo, E.G., Saavedra, J., Galindo, C., Fanning, C.M., 1998. The Pampean orogeny of the southern proto-Andes: evidence for Cambrian continental collision in the Sierras de Córdoba. In: Pankhurst, R.J., Rapela, C.W. (Eds.), The Proto-Andean Margin of Gondwana. Geological Society of London Special Publication. 142, pp. 181–217.
Rapela, C.W., Baldo, E.G., Pankhurst, R.J., Fanning, C.M., 2008. The Devonian Achala Batholith of the Sierras Pampeanas: F-rich, aluminous A-type granites. Actas VI South American Symposium on Isotope Geology, pp. 1–8 (San Carlos de Bariloche, Argentina).
Raymo, N.E., Ruddiman, W.F., 1992. Tectonic forcing of late Cenozoic climate. Nature 359, 117–122.
Román Ross, G., Kirschbaum, A.M., Ribeiro Guevara, S., Arribere, M.A., 1998. Procesos de meteorización en el granito de Achala, Sierra Grande de Córdoba: cambios químicos y mineralógicos. Rev. Asoc. Geol. Argent. 54 (4), 480–488.
Schedl, A., 1998. Log ratio methods for establishing a reference frame for chemical change. J. Geol. 106, 211–228.
Scott, K.M., Pain, C.F., 2009. Regolith Science. Springer-CSIRO Publishing, Dordrecht-Melbourne (461 pp.).
Sharma, A., Rajamani, V., 2000. Major element, REE and other trace element behaviour in amphibolite weathering under semiarid conditions in southern India. J. Geol. 108, 487–496.
Siegesmund, S., Steenken, A., Martino, R.D., Wemmer, K., López de Luchi, M.G., Frei, R., Presnyakov, S., Guereschi, A.B., 2010. Time constrains on the tectonic evolution of the Eastern Sierras Pampeanas (central Argentina). Int. J. Earth Sci. 99, 1199–1226.
Stallard, R.F., Edmond, J.M., 1983. Geochemistry of the Amazon 2. The influence of geology and weathering environment on the dissolved load. J. Geophys. Res. 88, 9671–9688.
Viles, H.A., 2013. Synergistic weathering processes. In: Shroeder, J., Pope, G. (Eds.), Treatise on Geomorphology. Academic Press, San Diego, pp. 12–16.
von Eynatten, H., Pawlowsky-Glahn, V., Egozcue, J.J., 2002. Understanding perturbation on the simplex: a simple method to better visualize and interpret compositional data in ternary diagrams. Math. Geol. 34, 249–257.
Woronow, A., Love, K.M., 1990. Quantifying and testing differences among means of compositional data suites. Math. Geol. 22 (7), 837–852.